

Dynamic crystallization and melting behavior of β -nucleated isotactic polypropylene polymerized with different Ziegler-Natta catalysts

Jian Kang · Jinggang Gai · Jingping Li · Shaohua Chen ·
Hongmei Peng · Bin Wang · Ya Cao · Huilin Li ·
Jinyao Chen · Feng Yang · Ming Xiang

Received: 6 November 2012 / Accepted: 28 December 2012 / Published online: 8 January 2013
© Springer Science+Business Media Dordrecht 2013

Abstract Large amount of work has been published on the dynamic crystallization and melting behavior of β -nucleated polypropylene (β -PP). However, the relationship between molecular structure and dynamic crystallization behavior of β -PP is still not clear. In this study, the dynamic crystallization and melting behavior of two β -nucleated isotactic polypropylene (β -iPP) with nearly same average isotacticity but different stereo-defect distribution, were studied by differential scanning calorimetry (DSC), wide angle X-ray diffraction (WAXD) and temperature modulated DSC (TMDSC). The results indicated that stereo-defect distribution of iPP can significantly influence the dependence of the β -crystal content and thermal stability on the cooling rate. NPP-A with less uniform stereo-defect distribution favors the crystallization at higher temperature region and the formation of β -crystal with high thermal stability in all cooling rates concerned, moreover, the β -crystal content is influenced by cooling rate; for NPP-B with more uniform distribution of stereo-defect, the crystallization temperature and the regular insertion of molecular chains can be reduced in a larger extent. NPP-B is more suitable for the formation of high proportion of β -crystal in both low and high cooling rates, meanwhile, the thermal stability of crystal is sensitive to the cooling rate. This work provides a new insight into the design of β -iPP in dynamic crystallization.

Keywords Isotactic polypropylene · β -crystal · Stereo-defect distribution · Dynamic crystallization · β - α recrystallization

Introduction

Polypropylene (PP) is one of the most widely used commodity polymers owing to its low manufacturing cost and rather versatile properties [1–3]. Semicrystalline iPP exhibits a very interesting polymorphic behavior, depending on the molecular structure [4], thermal history [5–9] and the presence of extraneous materials [10, 11]. Generally, four crystalline structures of iPP are known, including the monoclinic α -form, the trigonal β -form, the triclinic γ -form [12, 13], and the mesomorphic (smectic) form [14, 15].

Among the crystalline structures, the β -modification has received considerable interests because of several advantageous properties, for instance, high deformation temperature, high impact and tear strength, in comparison with that of α -iPP [16]. However, β -crystal has lower stability compared with the α -modification, and can only be formed under some critical conditions, e.g. quenching the melt to a certain temperature range [5], crystallization in a thermal gradient field [17], shearing or elongation of the melt during crystallization [18], vibration-induced crystallization [10], or the presence of β -nucleating agents [19–22]. Because of the lower stability and lower melting temperature of β -phase compared with α -modification, the crystalline phase transformation (β - α recrystallization) is a characteristic feature of β -iPP [23]. Researchers studied the β - α transformation of β -iPP during heating by combination of calorimetry measurement and simultaneous X-ray measurements [24, 25], and claimed that β - α recrystallization includes the temporary melting of the initial β -phase, the

J. Kang · J. Gai · J. Li · S. Chen · H. Peng · B. Wang · Y. Cao ·
H. Li · J. Chen · F. Yang (✉) · M. Xiang (✉)
State Key Laboratory of Polymer Materials Engineering,
Polymer Research Institute of Sichuan University, Chengdu,
Sichuan 610065, People's Republic of China
e-mail: yangfengscu@126.com
e-mail: xiangming45@hotmail.com

synchronized recrystallization into α -form, and the final melting of the α -form.

As one of the most important factor of the external crystallization conditions, cooling rate plays an important role in determining the crystallization of β -nucleated PP and has been extensively studied, great progress has been achieved. However, the influence of cooling rate on the crystallization and melting behavior of β -nucleated iPP is still under debate. Some researchers claimed that with lower cooling rate during dynamic crystallization, the proportion and thermal stability of the formed β -crystals were enhanced [26–31].

Meanwhile, some other authors held different point of views. Yu J et al. [32] studied the influence of cooling rate on the microstructure and thermal stability of iPP nucleated of a non-selective β -nucleating agent, and claimed that fast cooling rate is favorable for β -form iPP formation; with slower cooling rate, the stability of crystals was enhanced. Feng JC et al. [33] claimed that a higher proportion of β -phase in PPR containing β nucleating agent could be achieved under faster cooling rates. Ernesto et al. [4] suggested that, the sensitivities of Ziegler-Natta iPP and Metallocenic iPP to the cooling rate is quite different.

Moreover, it seems that iPP nucleated by compound α/β -nucleating agent systems has extraordinary response to the cooling rates. Researchers [34, 35] believed that in the dual additive system of iPP, the results not only depend on the nucleation efficiency and the relative content of the individual α and β nucleating agents, but also on the cooling rates employed. The nucleating behavior of the additives can be explained by the competitive nucleation.

The different results mentioned above might be attributed to the following reasons: Firstly, the nucleating mechanism, nucleating efficiency and selectivity of the nucleating agents used might be quite different from each other; Secondly, the molecular structure of the iPP applied in the studies, for instance, the molecular weight and its distribution, the defect concentration and its distribution, might also be different. Thirdly, the complicated DSC melting curves of β -iPP might confuse the obtained results [24]. Therefore, further investigations concerning the influence of the reasons mentioned above on the dynamic crystallization and melting behavior of β -nucleated iPP are still needed.

Due to the complexity in ZN-iPP polymerization, it is not easy to adjust the polymerization conditions and to obtain ZN-iPP with same average isotacticities, but different defect distributions. Currently, the effect of stereo-defect distribution on the dynamic crystallization and melting behavior of β -iPP is still not clear. The aim of this study is to investigate the influence of the stereo-defect distribution on the crystallization and melting behavior of β -iPP under dynamic crystallization conditions, in order to

provide a new insight for the structure–property relationship of β -iPP.

Experimental section

Materials and sample preparation

The preparation and microstructure characterization of the iPP used in this study was reported in the previous work [36]. The results of ^{13}C NMR, successive self-nucleation and annealing, and FT-IR had been discussed there in detail. A brief summary is given here.

The iPP samples studied (PP-A and PP-B) are iPP resins for biaxially oriented polypropylene (BOPP) film, which are polymerized by two different highly activity supported fourth generation Ziegler-Natta ($\text{TiCl}_4 = \text{MgCl}_2$) catalysts, ZN-A and ZN-B, respectively. The catalytic activity of ZN-A is higher than that of ZN-B. Other polymerization conditions, for instance, the hydrogen concentration, Al/Si ratio, temperature, pressure, of the two samples are the same. The average isotacticities of the samples are nearly same, but the stereo-defect distribution of PP-B is more uniform than PP-A. Other molecular parameters of the samples can be seen in the previous study [36].

The β -nucleating agent was a powder of metal salts (tradename NAB83) purchased from Guangzhou Chenghe (GCH) technology company and was a high efficiency selective β -crystal nucleating agent, and was used as received. However, we are not aware of the corresponding work about chemical structure and crystal information of NAB83 on the basis of the relevant patents.

The iPP pellets and NAB83 were mixed in the weight ratio of 100:2 and then extruded by a twin-screw extruder (SHJ-20, Nanjing Giant Machinery Co., Ltd, the screw speed is 30 rpm and the temperature of each part is 185, 195, 200, 200 °C, respectively) and pelletized to obtain a master batch. The master batch and iPP were mixed and extruded by twin-screw again to obtain β -iPP pellets. The concentration of nucleating agent was 0.05 wt.%. The obtained β -iPP samples were named as NPP-A and NPP-B.

For the WAXD, DSC and TMDSC measurements, the thin-sheet samples were prepared. The virgin polymers were firstly molded at 190 °C, 10 MPa for 5 min into thin sheets of 500 μm thickness, and then they were covered by glass slides and heated in the heating oven under 200 °C for 20 min to erase any previous thermal history. After that, two different thermal treatments were applied. One series of samples labeled “air cooling” were taken out of the heating oven and fast quenched down to room temperature. The second one named “oven cooling” were kept in the drying oven and slowly cooling down under the rate of about 2 °C/min.

Characterization

Differential scanning calorimetry (DSC)

All the calorimetric experiments were performed with a Mettler Toledo DSC1 differential scanning calorimeter (DSC), under nitrogen atmosphere (50 mL/min). The temperature scale calibration was performed using indium as a standard to ensure reliability of the data obtained. In order to ensure the homogeneity of samples and the good contact between sample and pan, the virgin polymer was molded at 190 °C, 10 MPa for 5 min into sheets of uniform thickness about 500 μm. Then 5 mg round samples were punched out of the sheets.

All the thermograms were fitted using Peakfit 4.12 software according to the manner in literatures [24], and the relative percentage crystallinities of α-crystal (α_c) and β-crystal (β_c) were estimated from DSC by the following expressions [37]:

$$\alpha_c = (1 - \lambda)_\alpha / [(1 - \lambda)_\beta + (1 - \lambda)_\alpha] \tag{1}$$

$$\beta_c = (1 - \lambda)_\beta / [(1 - \lambda)_\beta + (1 - \lambda)_\alpha] \tag{2}$$

where the degree of crystallinities (1-λ) associated with each phase, (1-λ)_α and (1-λ)_β, were calculated from the ratio ΔH/ΔHu. ΔH and ΔHu are the apparent and completely crystalline heats of fusion, respectively, and the values used for ΔHu for 100 % crystalline iPP, was 209 J g⁻¹ [38, 39].

The nonisothermal programmes involved melt crystallization at various cooling rates: 2, 5, 10, 20, 30 and 40 °C/min.

Temperature Modulated DSC (TMDSC)

The TMDSC melting curves of the samples were recorded with a Mettler Toledo DSC1 Instrument at V_h=1 °C/min, ±0.1 °C with 10 s modulation, ranging from 50 °C to 200 °C.

WAXD

Wide-angle X-ray diffraction (WAXD) patterns were recorded with a DX-1000 diffractometer. The wavelength of CuKα was λ=0.154 nm and the spectra were recorded in the 2θ range of 5–35°, a scanning rate of 2°/min, and a scanning step of 0.02°. The crystallite size L of each plane of samples was determined from the XRD using the Debye-Scherrer’s equation [40]:

$$L = 0.9\lambda / \beta \cos \theta \tag{3}$$

where λ is the X-ray wavelength of radiation used, θ is the Bragg angle and β is the full width of the diffraction line at half maximum (FWHM) intensity measured in radians.

The content of the β-crystal was determined according to standard procedures described in the literature [41], employing the following equation:

$$k_\beta = \frac{H_\beta(300)}{H_\beta(300) + H_\alpha(110) + H_\alpha(040) + H_\alpha(130)} \tag{4}$$

k_β denotes the relative content of β-crystal form (WAXD), H_α(110), H_α(040) and H_α(130) are the intensities of the strongest peaks of α-form attributed to the (110), (040) and (130) planes of monoclinic cell, respectively. H_β(300) is the intensity of the strongest (300) diffraction peak of the trigonal β-form.

Results and discussions

Nonisothermal crystallization and melting behavior

In nonisothermal crystallization kinetics, samples were firstly cooled from the melt to 30 °C at various cooling rate, 2, 5, 10, 20, 30 and 40 °C/min, then they were heated under the rate of 10 °C/min to 200 °C.

Crystallization behavior

The crystallization curves of the samples at different cooling rates are shown in Fig. 1. The crystallization parameters plotted as a function of the cooling rate are shown in Fig. 2, where T_{onset}-T_{endset} denotes to the crystallization peak width. The larger the T_{onset}-T_{endset}, the wider the crystallization temperature range.

In the previous study [36], it was found that the crystallization temperature of PP-A is obviously higher than that of PP-B. Interestingly, Fig. 2 shows that the T_c, T_{onset} and T_{endset} of NPP-A are still higher than that of NPP-B. On the other hand, the crystallization peak width T_{onset}-T_{endset} of NPP-A is larger than that of NPP-B at low cooling rates (2, 5, 10 and 20 °C/min); At high cooling rates (30 and 40 °C/min), the T_{onset}-T_{endset} of the samples become quite close.

Taking the stereo-defect distribution into consideration, the stereo-defect distribution of NPP-A is less uniform compared with NPP-B and contains more amount of high isotactic fractions. During the cooling process, these high isotactic fractions might begin to crystallize at relative high temperature, leading to a higher onset temperature of crystallization T_{onset} and a higher crystallization peak temperature T_c; On the other hand, NPP-A also contains fractions with medium and low isotacticity, which can only crystallize at relative lower temperature, resulting a relatively lower endset crystallization temperature T_{endset}. Finally, the crystallization peak width of NPP-A is larger than that of NPP-

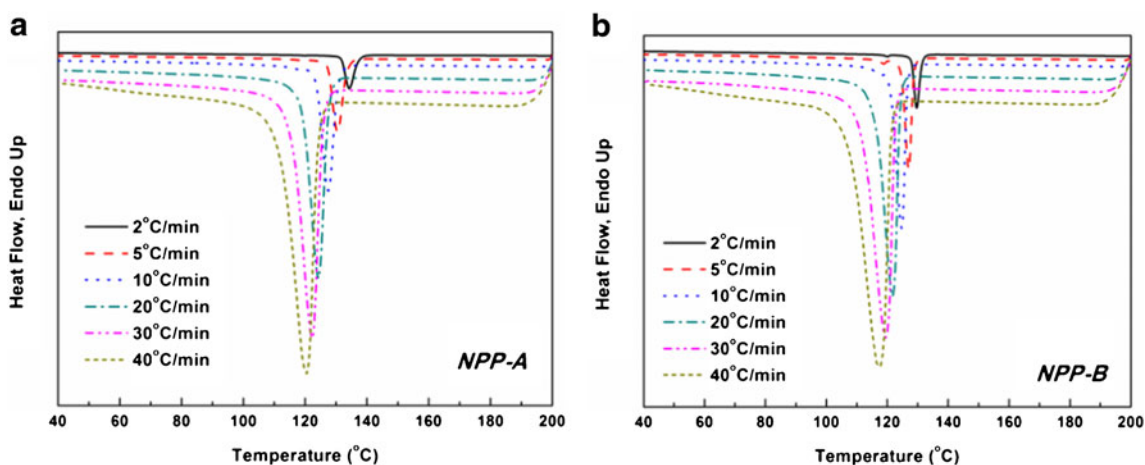


Fig. 1 Cooling curves of **a** NPP-A and **b** NPP-B at different cooling rates

B. As the cooling rates increases from 2 to 40 °C/min, the crystallization temperature difference between high and low isotactic fractions becomes less significant.

The accumulated curves of the relative degree of crystallinity as a function of crystallization time are calculated as shown in Fig. 3. The half crystallization time ($t_{1/2}$) of

nonisothermal crystallization, defined as the half period (i.e. 50 % crystallization), from the onset to endset of crystallization, is a direct measure of crystallization rate and is calculated as shown in Fig. 4.

Figure 4 reveals that at low cooling rates (2, 5, 10 and 20 °C/min), the $t_{1/2}$ of NPP-A is larger than that of NPP-B,

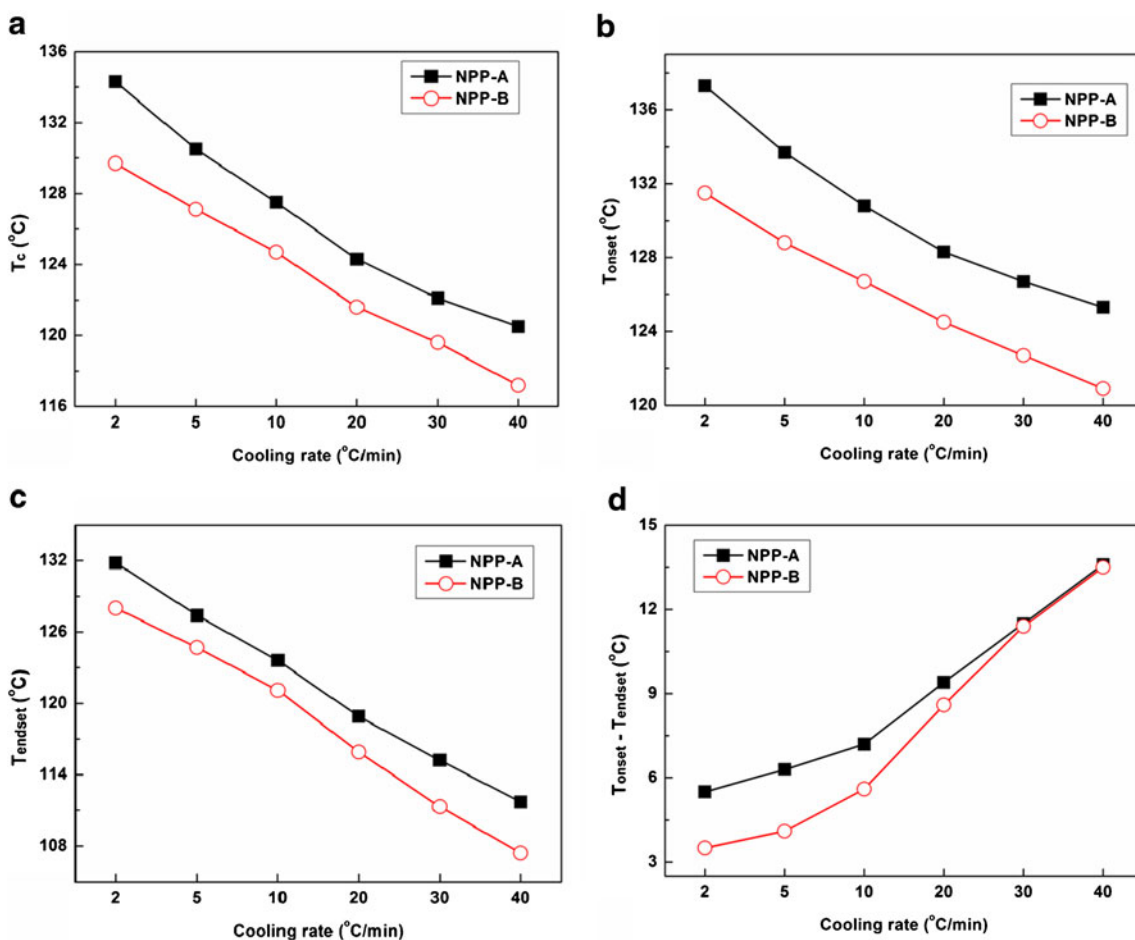


Fig. 2 Crystallization parameters of NPP-A and NPP-B at different cooling rates. **a** T_c , **b** T_{onset} , **c** T_{endset} and **d** $T_{onset} - T_{endset}$

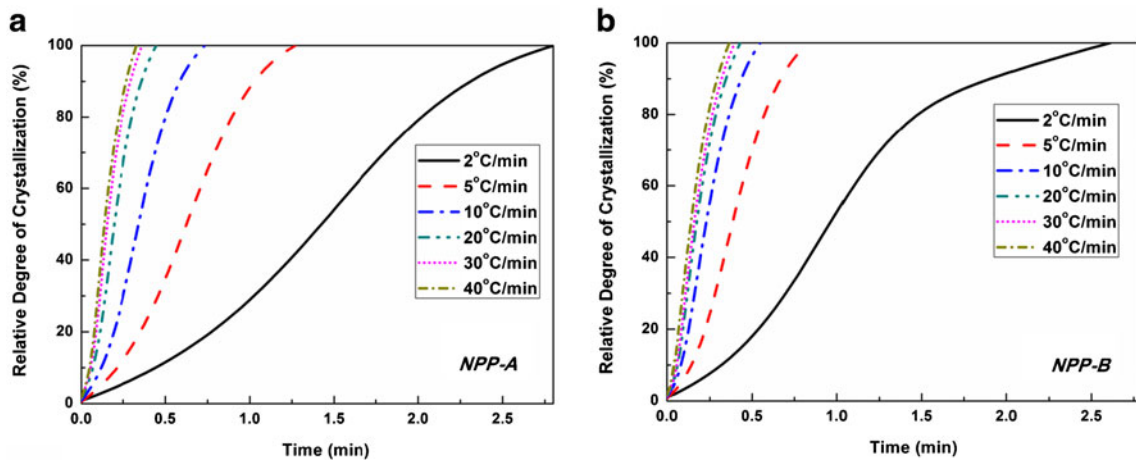


Fig. 3 Profiles of relative crystallinity as a function of crystallization time of **a** NPP-A and **b** NPP-B at different cooling rates

indicating that the time for NPP-A to finish the crystallization is longer than NPP-B; however, at high cooling rates (30 and 40 °C/min), the $t_{1/2}$ of the samples are quite close. The difference in $t_{1/2}$ of the samples is in correspondence with the crystallization peak width $T_{onset}-T_{endset}$ results. During dynamic crystallization at low cooling rates, it is easier for NPP-A to crystallize at higher temperature compared with NPP-B, meanwhile, it takes less time for NPP-B to finish the crystallization.

Melting behavior

The melting curves at the heating rate of 10 °C/min are shown in Fig. 5. According to Fig. 5, the relative percentages of crystallinity of α -crystal α_c and β -crystal β_c , the degree of crystallinity of α -crystal $(I-\lambda)_\alpha$ and β -crystal $(I-\lambda)_\beta$ are calculated as plotted in Fig. 6.

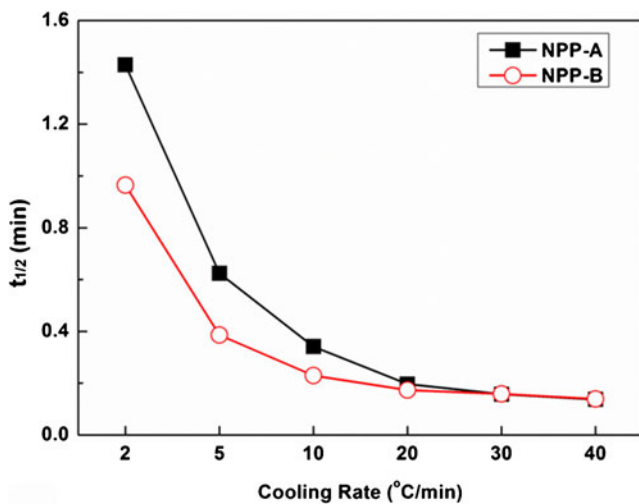


Fig. 4 The half crystallization time $t_{1/2}$ of NPP-A and NPP-B at different cooling rates

As can be seen from Fig. 6, when the cooling rate increases from 2 to 40 °C/min, for NPP-A, the β_c increases from 6.5 to 28.9 % and the $(I-\lambda)_\beta$ increases from 3.4 to 13.6 %; however, for NPP-B, the β_c and $(I-\lambda)_\beta$ decrease from 93.3 % and 41.6 % to 68.9 % and 35.2 %, respectively. Meanwhile, it can be observed that as the cooling rate increases, the α_c and $(I-\lambda)_\alpha$ of NPP-A decrease gradually, and these parameters of NPP-B increase gradually.

The results above reveal that the β -crystal content of NPP-B is significantly higher than that of NPP-A at the same cooling rate, and NPP-B is more favorable for the formation of high proportion of β -crystal. Moreover, the cooling rate dependence for β -crystal content obtained from DSC heating curves of NPP-A and NPP-B are quite different.

During the melting of β -iPP, the β - α recrystallization usually takes place, which results in the overlap of the endotherm of the melting β -form, the crystallization exotherm from molten amorphous into α -form and endotherm of the final melting of α -form, consequently confuses the β -crystal content calculated from the final DSC melting curve. Since it is usually not possible for one kind of polymer to have two contrary cooling rate dependences, the different cooling rate dependences of β -crystal content between NPP-A and NPP-B might be attributed to the different thermal stability of the formed β -crystal.

DSC measurement after elimination of the β - α recrystallization

Varga et al. [5, 25, 41–43] reported the complex melting and recrystallization behavior of β -iPP, and claimed that the melting behavior strongly depends on the thermal post history of the samples. During the partial melting of the β -crystal, β -iPP cooled below the critical temperature ($T_R^* = 100^\circ\text{C}$) recrystallizes into the α -phase, leading to an enhanced

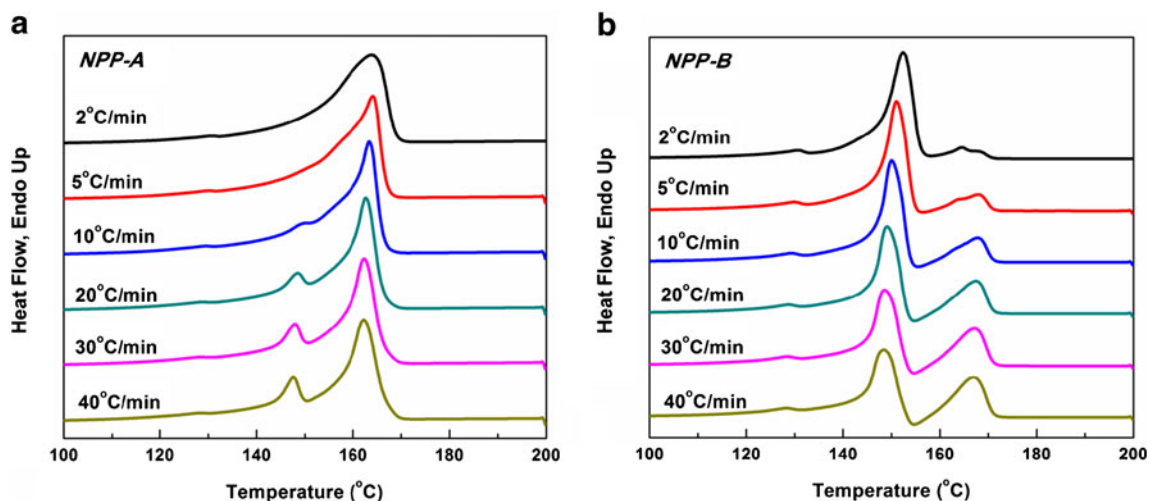


Fig. 5 Melting curves of **a** NPP-A and **b** NPP-B at different cooling rates

apparent α -content determined from the DSC melting curves. On the contrary, if β -iPP is not cooled down below T_R^* after crystallization, no $\beta\alpha$ -recrystallization occurs during heating, and a separate β -melting peak appears on the DSC trace. In this way, the polymorphic composition of β -nucleated iPP can be determined from the DSC melting curves [5, 41, 43, 44].

In this study, the end temperature of recooling (T_R^*) was set to $T_R^* = 120^\circ\text{C}$ in the subsequent series of experiment (second run), in order to eliminate the disturbing effect of β - α recrystallization. The consequent melting curves after cooling at different cooling rates (2, 5, 10, 20, 40 $^\circ\text{C}/\text{min}$) are recorded as shown in Fig. 7.

According to Fig. 7, the relative percentages of crystallinity of α -crystal α_c and β -crystal β_c , the degree of crystallinity of α -crystal $(1-\lambda)_\alpha$ and β -crystal $(1-\lambda)_\beta$ are calculated and plotted in Fig. 8, as a function of cooling rate.

After elimination of β - α recrystallization, the β -peak profile of NPP-B gradually shifts to lower temperature

region as the cooling rate increases, suggesting a decrease of the structural stability of the crystal. However, this phenomenon is hardly observed for NPP-A, indicating that the crystal structural stability of NPP-B has less dependence on the cooling rate, and is higher than NPP-A.

On the other hand, the β -crystal content of NPP-A increases gradually as the cooling rate increases, which is in accord with the results from the samples recooled to room temperature, revealing that for NPP-A, the thermal stability of the β -crystal is high, and the β - α recrystallization is relatively difficult to occur. However, after the exclusion of β - α recrystallization, the β -crystal content is still low, indicating that high content of β -crystal can hardly be formed in NPP-A.

Meanwhile, high content of β -crystal is obtained from NPP-B in all cooling rates used, and the β -content of remains nearly unchanged as the cooling rate increases, suggesting that the cooling rate has little influence on the exact β -crystal content of NPP-B; however, it can significantly affect

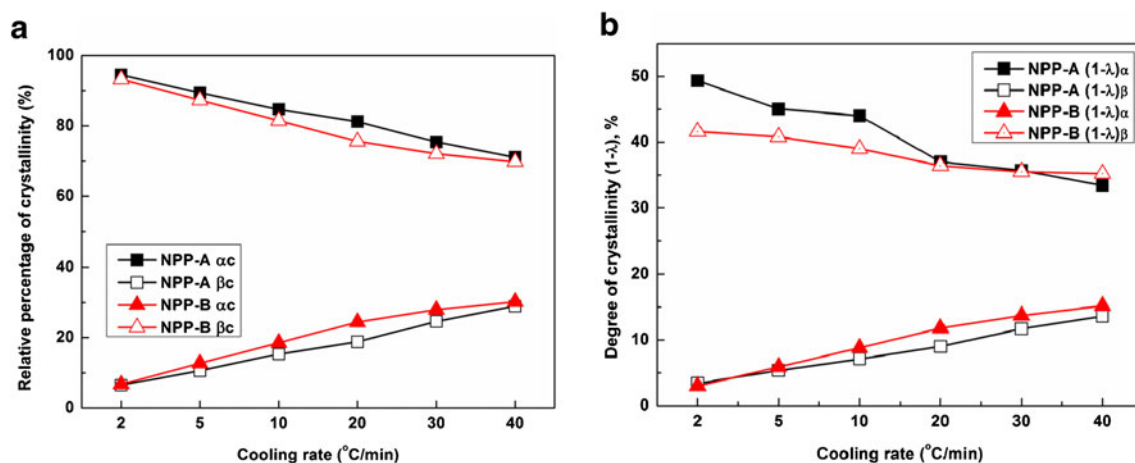


Fig. 6 **a** Relative percentages of crystallinity of α -phase α_c and β -phase β_c and **b** the degrees of crystallinity of α -phase $(1-\lambda)_\alpha$ and β -phase $(1-\lambda)_\beta$ of NPP-A and NPP-B as a function of cooling rate. All the values were evaluated from heating curves in Fig. 5

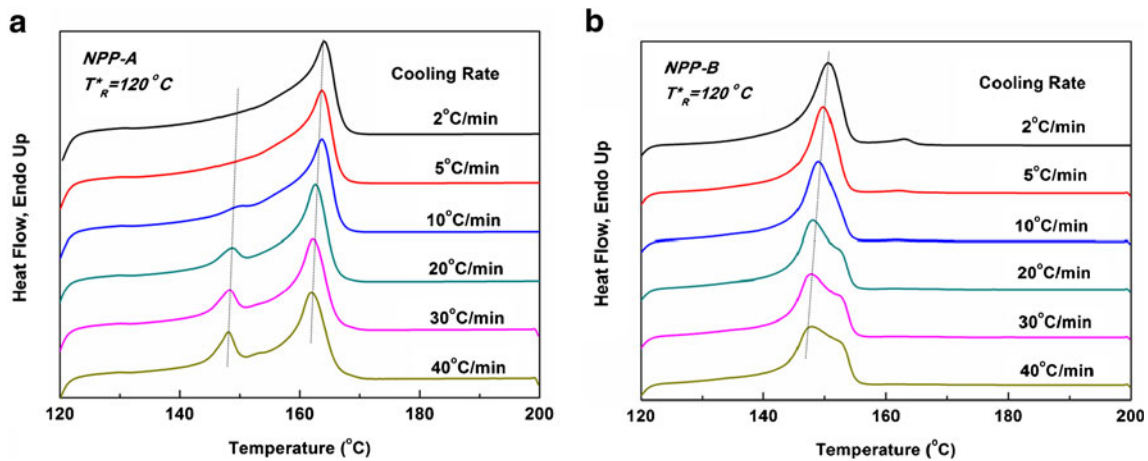


Fig. 7 Subsequent melting curves of **a** NPP-A and **b** NPP-B after recooled under different cooling rate to the end temperature of $T_R^* = 120^\circ\text{C}$

the thermal stability of the β -crystal. The higher the cooling rate, the lower the thermal stability of the β -crystal, and the larger extent of β - α recrystallization during heating.

Characterization of the air-cooling and oven-cooling samples

In order to understand the interesting crystallization behavior of NPP-A and NPP-B fully, a combination analysis of WAXD, DSC and TMDSC is applied. Two different thermal treatments were applied to the samples. One series of samples labeled “air cooling” were taken out of the drying oven and fast quenched down to room temperature. The second one named “oven cooling” were kept in the drying oven and slowly cooling down under the rate of about $2^\circ\text{C}/\text{min}$.

DSC analysis

The melting curves of the samples at the heating rate of $10^\circ\text{C}/\text{min}$ are shown in Fig. 9, and β_c , $(I-\lambda)_\beta$, α_c and $(I-\lambda)_\alpha$ are

calculated using Peakfit 4.12 as shown in Table 1. It should be noted that in Fig. 9(a), the melting curves of NPP-A and NPP-B exhibit multiple overlapped peaks, which is attributed to the presence of β -crystal with different thicknesses.

As can be seen from Fig. 9 and Table 1, for air cooling samples (rapid cooling), a β -crystal content of less than 40 % has formed in both NPP-A and NPP-B; for oven cooling samples however, the β -crystal peak of NPP-A is very small, but a high β -crystal content of 81.0 % has formed in NPP-B. These phenomenon are in accord with the findings in the DSC nonisothermal crystallization analysis above.

WAXD analysis

The WAXD profiles of the samples are shown in Fig. 10. The crystalline parameters calculated from Fig. 10 are shown in Table 2.

Since the WAXD is performed under room temperature, the confusion of β - α phase transformation can be excluded. As can be seen from Fig. 10 and Table 2, the crystallite sizes

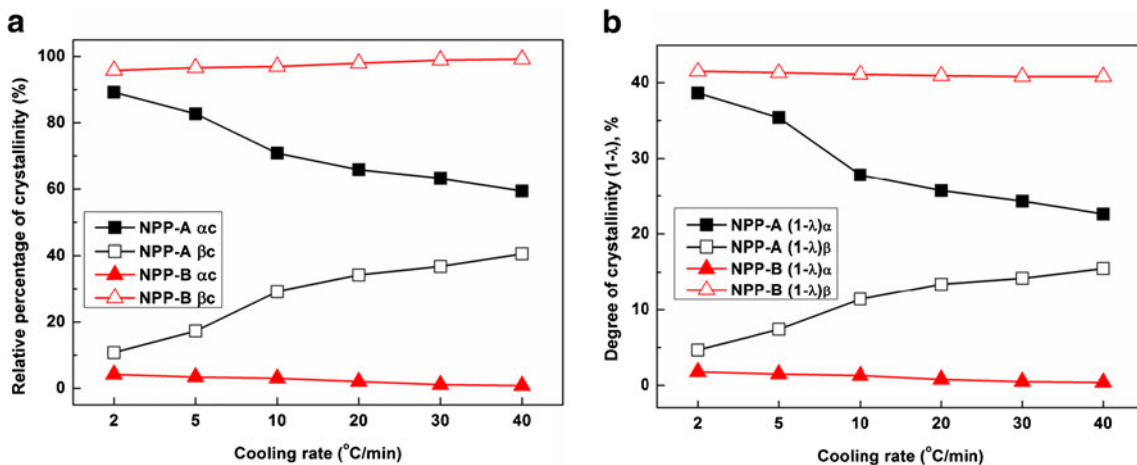


Fig. 8 **a** Relative percentages of crystallinity of α -phase α_c and β -phase β_c and **b** the degrees of crystallinity of α -phase $(I-\lambda)_\alpha$ and β -phase $(I-\lambda)_\beta$ of NPP-A and NPP-B as a function of cooling rate. All the values were evaluated from heating curves in Fig. 7

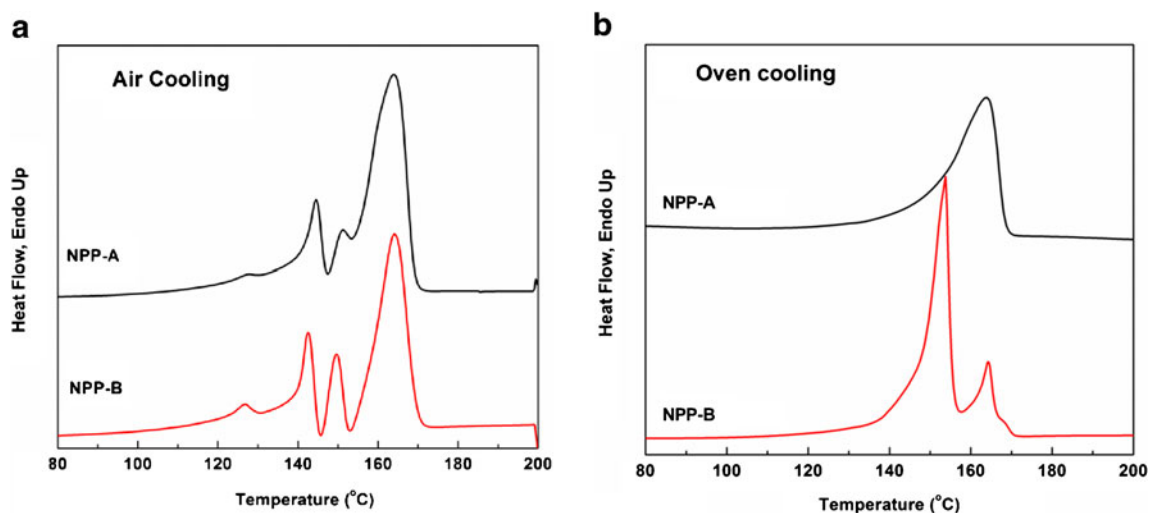


Fig. 9 DSC heating curves of the β -iPP samples under different cooling rates. **a** Air cooling (about 80 °C/min), **b** Oven cooling (about 2 °C/min)

of each plane of NPP-A is larger than NPP-B under the same thermal condition;

On the other hand, for air-cooling samples, a sharp peak at $\theta=16^\circ$, characteristic of $\beta(300)$ plane, can be found from both NPP-A and NPP-B, and the k_β of NPP-B (83.4 %) is obviously higher than that of NPP-A (44.3 %). Compared with the results obtained from DSC (Fig. 9 and Table 1), for NPP-A, the β_c (34.9 %) is close to k_β (44.3 %), suggesting that the β -crystal thermal stability of NPP-A is high; however, for NPP-B, the β_c (39.8 %) is much smaller from k_β (83.4 %), suggesting that the thermal stability of NPP-B is much lower than that of NPP-A, which might be attributed to the molecular structure differences between PP-A and PP-B.

On the other hand, as the cooling rate increases, the β -crystal content k_β of NPP-A increases significantly from 11.5 % to 44.3 %, meanwhile, the k_β of NPP-B remains more than 80.0 % and is almost unchanged, which is in accord with the DSC analysis of $T_R^* = 120^\circ\text{C}$ recooled samples.

Temperature modulated DSC (TMDSC) analysis

In order to gain further insight to the nature of the crystallization behavior of NPP-A and NPP-B, TMDSC is

performed on the samples as shown in Fig. 11. Compared with conventional DSC, TMDSC has been shown to be a useful technique to clarify the multiple transitions of polymers [45–50]. In the measurement, the obtained total heat flow, approximately equivalent to that from a conventional DSC, can be divided into a (capacity-related) reversible heat flow and a (kinetic) nonreversible heat flow [51].

Air cooling

Oven cooling

Generally, crystallization and enthalpy relaxation (or recovery) appear only in the nonreversible signal, whereas melting occurs in both reversible and nonreversible signals [48,

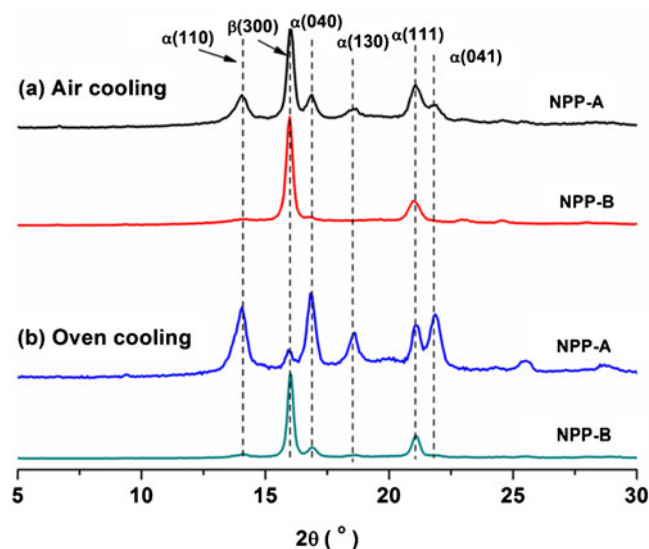


Fig. 10 WAXD profiles of the β -iPP samples under different cooling rates

Table 1 Melting parameters of β -iPP samples under different cooling rates

Thermal condition	Sample	β_c (%)	α_c (%)	X_β (%)	X_α (%)
Air cooling	PP-A + NAB83	34.9	65.1	14.8	27.5
	PP-B + NAB83	39.8	59.9	16.8	25.2
Oven cooling	PP-A + NAB83	8.9	91.1	4.4	45.2
	PP-B + NAB83	81.0	19.0	39.3	9.2

Table 2 WAXD parameters of β -iPP samples under slow cooling rate (2 °C/min)

Parameters	Sample		$\alpha(110)$	$\beta(300)$	$\alpha(040)$	$\alpha(130)$	$\alpha(111)$
L (nm)	Air cooling	NPP-A	118	294	196	157	161
		NPP-B	66	287	192	–	159
	Oven cooling	NPP-A	144	340	215	208	214
		NPP-B	118	296	213	191	261
k_{β} (%)	Air cooling	NPP-A			44.3		
		NPP-B			83.4		
	Oven cooling	NPP-A			11.5		
		NPP-B			81.6		

51–54]. Namely, only melting appears on the reversing signal. Therefore, the reversing signal can be used to analysis the separated melting behavior of the sample, including the melting of β -phase and the final melting of the α -phase. For air cooling samples (Fig. 11(a and b)), only a small β -crystal melting peak emerges in the reversing and total signal of NPP-A, suggesting that only a small amount of β -crystal has formed; meanwhile, a more obvious β -crystal melting peak appears in the reversing signal of NPP-B. However, due to the

low thermal stability of NPP-B, the β - α recrystallization exothermic peaks is overlapped with the endothermic β -crystal melting peak, and finally decreases the intensity of the β -crystal melting peak in the total signal.

Figure 11(c and d) reveal that for oven cooling samples, the total signal and the reversing signal of NPP-A are quite similar, which might indicate that the crystal structure formed is quite stable. However, the β -melting peak is quite ambiguous, which can hardly be observed; For NPP-B, a

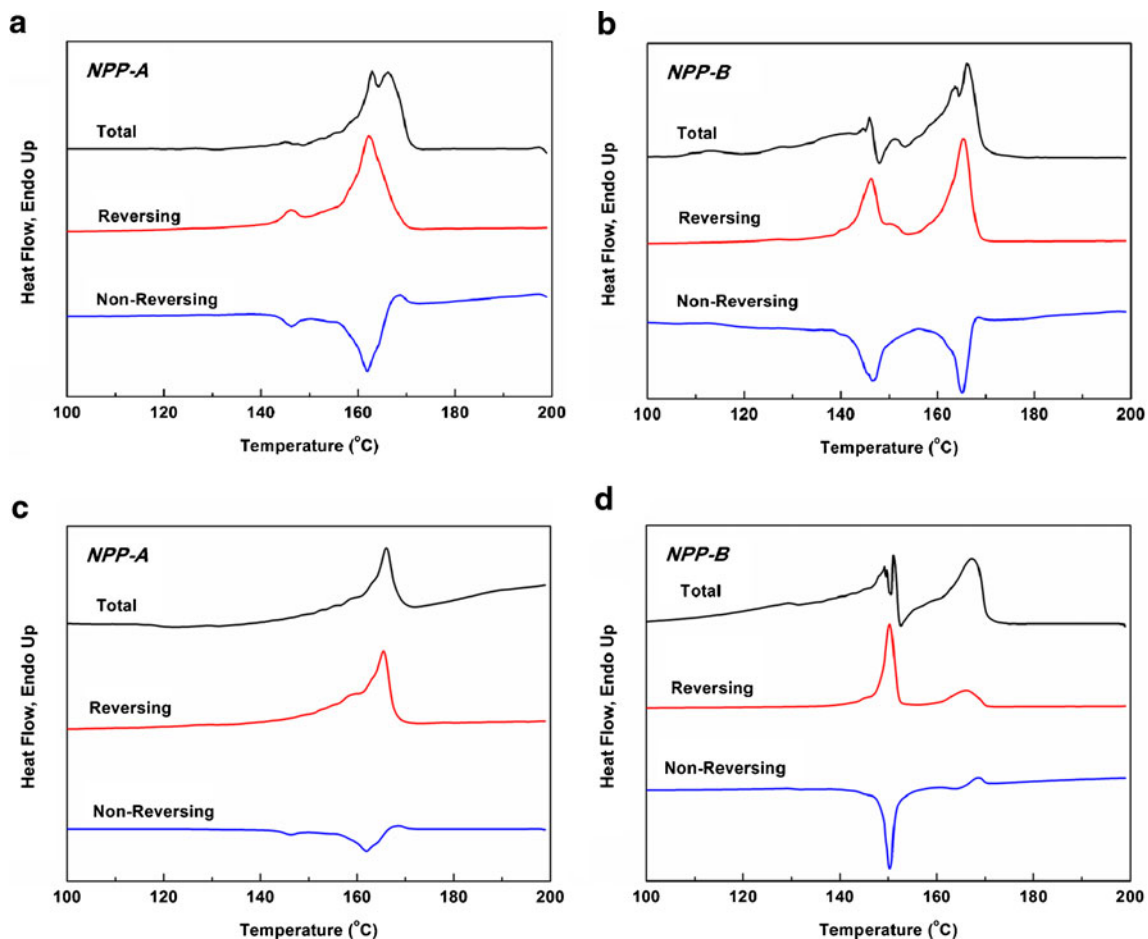


Fig. 11 TMDSC melting curves of NPP-A and NPP-B at 1 °C/min. Air cooling samples of **a** NPP-A and **b** NPP-B, and Oven cooling samples of **c** NPP-A and **d** NPP-B

sharp β -crystal melting peaks can be found on the reversing signal, indicating the formation of a large amount of β -crystal. A large β -crystal melting peak can also be found in the total signal, which might be due to the enhancement of the β -crystal thermal stability.

The results above demonstrate that, the stereo-defect distribution significantly influences the dynamic crystallization behavior of β -nucleated iPP.

For NPP-A, the less uniform distribution of stereo-defect results in the high crystallization temperature, which might be too high for the formation of β -crystal; On the other hand, chains movement and regular insertion of the molecular chains during crystallization is quite strong, resulting in a strong tendency for the formation of α -phase and high thermal stability of the crystal. High cooling rate can lower the crystallization temperature and reduce the tendency of α -phase formation, and therefore enhance β -crystal content. Anyway, it is hard for NPP-A to produce high proportion of β -crystal.

For NPP-B, the more uniform distribution of stereo-defects decreases both the crystallization temperature and the regular insertion of molecular chains during the crystallization, which might be more suitable for the formation of β -crystal. Therefore, under all cooling rate studied, a high proportion of β -crystal can be formed, and it seems that the cooling rate has little influence on the β -crystal content; On the other hand, the thermal stability of β -crystal is greatly influenced by the cooling rate. The lower the cooling rate, the higher the thermal stability of the β -crystal.

Conclusions

In this study, the dynamic crystallization and melting behavior of two β -nucleated ZN-iPP with nearly same average isotacticity but different stereo-defect distribution, were investigated by means of DSC, WAXD and TMDSC. This study takes the stereo-defect distribution into consideration, and provides novel insight in designing the β -nucleated ZN-iPP. The following conclusions can be drawn:

The stereo-defect distribution of iPP can significantly influence the crystallization and melting behavior during dynamic crystallization. ZN-iPP with different stereo-defect distributions can exhibit different dependence on the cooling rate.

For the ZN-iPP in this study, a more uniform distribution of stereo-defect can decrease the crystallization temperature and the regular insertion of molecular chains in a larger extent, which is more suitable for the formation of high proportion of β -crystal in both low and high cooling rates; meanwhile, the thermal stability of crystal is sensitive to the cooling rate: the higher the cooling rate, the lower the thermal stability of the crystal. On the contrary, a less uniform stereo-defect distribution favors the formation of crystal with high thermal stability

in all cooling rates concerned; the β -crystal content greatly depends on the cooling rate applied: the faster the cooling rate, the higher the β -crystal content.

Generally, both the stereo-defect distribution and cooling rate will influence the formation of β -crystal, it should be carefully to choose proper ZN-iPP resins and crystallization conditions during the producing to β -iPP.

Acknowledgment We express our sincerely thanks to the Program for New Century Excellent Talents in University (NCET-10-0562).

References

1. Haque M, Islam S, Islam N (2012) Preparation and characterization of polypropylene composites reinforced with chemically treated coir. *J Polym Res*. doi:10.1007/s10965-012-9847-z
2. Zhu L, Xu X, Sheng J (2011) The effect of stretching on the morphological structures and mechanical properties of polypropylene and poly(ethylene-co-octene) blends. *J Polym Res* 18 (6):2469–2475
3. Kang J, Cao Y, Li HL, Li JP, Chen SH, Yang F, Xiang M (2012) *J Polym Res*. doi:10.1007/s10965-012-0037-9
4. Krache R, Benavente R, Lopez-Majada JM, Perena JM, Cerrada ML, Perez E (2007) Competition between α , β , and γ Polymorphs in a β -Nucleated Metallocenic Isotactic Polypropylene. *Macromolecules* 40(19):6871–6878
5. Varga J (2002) β -Modification of Isotactic Polypropylene: preparation, structure, processing, properties, and application. *J Macromol Sci, Part B: Polym Phys* 41(4):1121–1171
6. Lorenzo AT, Arnal ML, Muller AJ, Lin MC, Chen HL (2011) SAXS/DSC analysis of the lamellar thickness distribution on a SSA thermally fractionated model polyethylene. *Macromol Chem Phys* 212(18):2009–2016
7. Muller AJ, Arnal ML (2005) Thermal fractionation of polymers. *Prog Polym Sci* 30(5):559–603
8. Lorenzo AT, Muller AJ (2008) Estimation of the nucleation and crystal growth contributions to the overall crystallization energy barrier. *J Polym Sci Part B: Polym Phys* 46(14):1478–1487
9. Lorenzo AT, Arnal ML, Sanchez JJ, Muller AJ (2006) Effect of annealing time on the self-nucleation behavior of semicrystalline polymers. *J Polym Sci Part B: Polym Phys* 44(12):1738–1750
10. Kang J, Chen JY, Cao Y, Li HL (2010) Effects of ultrasound on the conformation and crystallization behavior of isotactic polypropylene and β -isotactic polypropylene. *Polymer* 51(1):249–256
11. Xu JZ, Liang YY, Huang HD, Zhong GJ, Lei J, Chen C, Li ZM (2012) Isothermal and nonisothermal crystallization of isotactic polypropylene/graphene oxide nanosheet nanocomposites. *J Polym Res*. doi:10.1007/s10965-012-9975-5
12. Dimeska A, Phillips PJ (2006) High pressure crystallization of random propylene–ethylene copolymers: α – γ Phase diagram. *Polymer* 47(15):5445–5456
13. Chen JY, Cao Y, Li HL (2010) The effect of propylene–ethylene copolymers with different comonomer content on melting and crystallization behavior of polypropylene. *J Appl Polym Sci* 116 (2):1172–1183
14. Mileva D, Androsch R, Zhuravlev E, Schick C, Wunderlich B (2012) Homogeneous nucleation and mesophase formation in glassy isotactic polypropylene. *Polymer* 53(2):277–282
15. Androsch R, Di Lorenzo ML, Schick C, Wunderlich B (2010) Mesophases in polyethylene, polypropylene, and poly(1-butene). *Polymer* 51(21):4639–4662

16. Grein C (2005) Toughness of neat, rubber modified and filled β -nucleated polypropylene: from fundamentals to applications. *Adv Polym Sci* 188:43–104
17. Shangguan Y, Song Y, Peng M, Li B, Zheng Q (2005) Formation of β -crystal from nonisothermal crystallization of compression-molded isotactic polypropylene melt. *Eur Polym J* 41(8):1766–1771
18. Zhang B, Chen J, Ji F, Zhang X, Zheng G, Shen C (2012) Effects of melt structure on shear-induced β -cylindrites of isotactic polypropylene. *Polymer* 53(8):1791–1800
19. Bai H, Luo F, Zhou T, Deng H, Wang K, Fu Q (2011) New insight on the annealing induced microstructural changes and their roles in the toughening of β -form polypropylene. *Polymer* 52(10):2351–2360
20. Wang YR, Ni QL, Liu ZH, Zou JD, Zhu XS (2011) Grafting modification and properties of polypropylene with pentaerythritol tetra-acrylate. *J Polym Res* 18(6):2185–2193
21. Lu QL, Dou Q (2009) β -crystal formation of isotactic polypropylene induced by N, N'-dicyclohexylsuccinamide. *J Polym Res* 16(5):555–560
22. Cheng S, Wen DJ, Wu GQ (2009) Preparation and characterization of fluorinated polypropylene by reactive extrusion with fluorinated acrylate. *J Polym Res* 16(3):271–278
23. Cho K, Nabi Saheb D, Yang H, Kang BI, Kim J, Lee SS (2003) Memory effect of locally ordered α -phase in the melting and phase transformation behavior of β -isotactic polypropylene. *Polymer* 44(14):4053–4059
24. Yamamoto Y, Inoue Y, Onai T, Doshu C, Takahashi H, Uehara H (2007) Deconvolution analyses of differential scanning calorimetry profiles of β -Crystallized polypropylenes with synchronized X-ray measurements. *Macromolecules* 40(8):2745–2750
25. Varga J, Menyhard A (2007) Effect of solubility and nucleating duality of N,N'-Dicyclohexyl-2,6-naphthalenedicarboxamide on the supermolecular structure of isotactic polypropylene. *Macromolecules* 40(7):2422–2431
26. Zhang RH, Shi DA, Tsui CP, Tang CY, Tjong SC, Li RKY (2011) The formation of β -polypropylene crystals in a compatibilized blend of isotactic polypropylene and polyamide-6. *Polym Eng Sci* 51(2):403–410
27. Zhiyong W, Wanxi Z, Guangyi C, Jicai L, Shu Y, Pei W, Lian L (2010) Crystallization and melting behavior of isotactic polypropylene nucleated with individual and compound nucleating agents. *J Therm Anal Calorim* 102(2):775–783
28. Liu M, Guo B, Du M, Chen F, Jia D (2009) Halloysite nanotubes as a novel β -nucleating agent for isotactic polypropylene. *Polymer* 50(13):3022–3030
29. Xiao W, Wu P, Feng J, Yao R (2009) Influence of a novel β -nucleating agent on the structure, morphology, and nonisothermal crystallization behavior of isotactic polypropylene. *J Appl Polym Sci* 111(2):1076–1085
30. Zhang YF (2008) Crystallization and melting behaviors of isotactic polypropylene nucleated with compound nucleating agents. *J Polym Sci Part B: Polym Phys* 46(9):911–916
31. Shen CY, Zhou YG, Zheng GQ, Liu CT, Chen JB, Li Q (2008) Stretching-induced β -crystal of iPP: Influence of stretching ratio. *Polym Eng Sci* 48(12):2454–2458
32. Dong M, Guo Z, Su Z, Yu J (2011) The effects of crystallization condition on the microstructure and thermal stability of isotactic polypropylene nucleated by β -form nucleating agent. *J Appl Polym Sci* 119(3):1374–1382
33. Xiao W, Feng J (2010) Comparative investigation on crystallization conditions dependence of polymorphs composition for β -nucleated propylene/ethylene copolymer and propylene homopolymer. *J Appl Polymer Sci* 117(6):3247–3254
34. Zhao S, Xin Z (2010) Nucleation characteristics of the α/β compounded nucleating agents and their influences on crystallization behavior and mechanical properties of isotactic polypropylene. *J Polym Sci Part B: Polym Phys* 48(6):653–665
35. Naffakh M, Marco C, Ellis G (2011) Novel Polypropylene/Inorganic Fullerene-like WS₂ nanocomposites containing a β -Nucleating agent: dynamic crystallization and melting behavior. *J Phys Chem B* 115(37):10836–10843
36. Kang J, Yang F, Wu T, Li H, Liu D, Cao Y, Xiang M (2012) Investigation of the stereodeflect distribution and conformational behavior of isotactic polypropylene polymerized with different Ziegler–Natta catalysts. *J Appl Polym Sci* 125(4):3076–3083
37. Marco C, Gomez MA, Ellis G, Arribas JM (2002) Activity of a β -nucleating agent for isotactic polypropylene and its influence on polymorphic transitions. *J Appl Polym Sci* 86(3):531–539
38. Turner-Jones A, Aizlewood J, Beckett D (1964) *Makromol Chem* 75:134
39. Li JX, Cheung WL, Jia D (2005) A study on the heat of fusion of β -polypropylene. *Polymer* 40(5):1219–1222
40. Scherrer P (1918) Bestimmung der Grosse und der inneren Struktur von Kolloidteilchen mittels Röntgenstrahlen. *Gottinger Nachrichten* 26:98–100
41. Menyhard A, Varga J, Molnar G (2006) Comparison of different-nucleators for isotactic polypropylene, characterisation by DSC and temperature-modulated DSC (TMDSC) measurements. *J Therm Anal Calorim* 83(3):625–630
42. Varga J (1986) Melting memory effect of the β -modification of polypropylene. *J Therm Anal Calorim* 31(1):165–172
43. Varga J (1995) Crystallization, melting and supermolecular structure of isotactic polypropylene. *Polypropylene Struct Blends Compos* 1:56–115
44. Horvath Z (2010) The effect of molecular mass on the polymorphism and crystalline structure of isotactic polypropylene. *eXPRESS Polym Lett* 4(2):101–114
45. Sharon Xin L, Cebe P (1996) Effects of annealing on the disappearance and creation of constrained amorphous phase. *Polymer* 37(21):4857–4863
46. Song M (2001) Rigid amorphous phase and low temperature melting endotherm of poly(ethylene terephthalate) studied by modulated differential scanning calorimetry. *J Appl Polym Sci* 81(11):2779–2785
47. Xu H, Cebe P (2004) Heat capacity study of isotactic polystyrene: dual reversible crystal melting and relaxation of rigid amorphous fraction. *Macromolecules* 37(8):2797–2806
48. Wang X, Zhou J, Li L (2007) Multiple melting behavior of poly(butylene succinate). *Eur Polym J* 43(8):3163–3170
49. Righetti MC, Di Lorenzo ML, Tombari E, Angiuli M (2008) The low-temperature endotherm in Poly(ethylene terephthalate): partial melting and rigid amorphous fraction mobilization. *The J Phys Chem B* 112(14):4233–4241
50. Di Lorenzo ML, Righetti MC, Cocca M, Wunderlich B (2010) Coupling between crystal melting and rigid amorphous fraction mobilization in Poly(ethylene terephthalate). *Macromolecules* 43(18):7689–7694
51. Okazaki I, Wunderlich B (1996) Modulated differential scanning calorimetry in the glass transition region. V. Activation energies and relaxation times of poly(ethylene terephthalate)s. *J Polym Sci Part B: Polym Phys* 34(17):2941–2952
52. Androsch R, Wunderlich B (2001) Reversible crystallization and melting at the lateral surface of isotactic polypropylene crystals. *Macromolecules* 34(17):5950–5960
53. Hu W, Albrecht T, Strobl G (1999) Reversible surface melting of PE and PEO crystallites indicated by TMDSC. *Macromolecules* 32(22):7548–7554
54. Genovese A, Shanks R (2004) Crystallization and melting of isotactic polypropylene in response to temperature modulation. *J Therm Anal Calorim* 75(1):233–248